2025 IMEKO TC26 International Conference on
Metrology for Archaeology and Cultural Heritage
Bergamo, Italy, October 15-17, 2025

XRD and PCA analysis of historic mortars from the Venetian Fortress of Bergamo (Italy)

Renato Pelosato *, Isabella Natali-Sora *, Virna Maria Nannei and Giulio Mirabella Roberti

Dipartimento di Ingegneria e Scienze Applicate, Università degli studi di Bergamo.
Via Marconi 5, 24044 Dalmine(BG), Italy.
*renato.pelosato@unibg.it; *isabella.natali-sora@unibg.it

***Abstract* – Mortars from the 16th-century Venetian Fortress of Bergamo (Italy) were investigated using X-ray diffraction (XRD). Samples were taken from the bastions of San Pietro and Valverde, areas affected by severe degradation and targeted in a recent conservation initiative. XRD qualitative phase analysis and semi-quantitative analysis were performed on 59 samples collected from 9 cores extracted at different locations. XRD analysis identified calcite, hydrocalumite- and hydrotalcite-type compounds, brucite, aragonite, plombierite, and a substantial amorphous fraction in the binder, while aggregates consist mainly of quartz and carbonate-rich sands. The large dataset of abundances of phases in the 59 samples was analyzed via principal component analysis (PCA). PCA results indicate a homogeneous distribution of mineral phases across the dataset, with no significant clustering by depth or sampling location, supporting the interpretation of a consistent binder composition throughout the investigated sections.**

I. INTRODUCTION

In 1561, the Serenissima Repubblica di Venezia began the challenging task of constructing a fortress to defend Bergamo, its westernmost city, from the rival Ducato di Milano. This fortress, with 11 bulwarks, 5 platforms, 4 main gates, and a perimeter of approximately 5 kilometres, has become a landmark in Bergamo (Figure 1) [1]. During the 19th century, the fortress underwent modifications to allow public access to the ramparts and to connect Porta Sant'Agostino with Porta Sant'Alessandro by road, while retaining its original structure. A small section of the San Pietro bulwark was demolished in 1908 to make way for Via Beltrami [2]. Given the historical and urban significance of the site for Bergamo, the municipality nominated the fortress for the World Heritage List as part of the transnational site "The Venetian Works of Defence between 16th and 17th centuries: Stato da Terra - Western Stato da Mar" acknowledged in 2017 [3]. In 2015, to support the UNESCO nomination, Bergamo's municipality, responsible for maintenance, collaborated with the University of Bergamo and the volunteer organisation Orobicambiente OdV to develop a conservation strategy to ensure proper upkeep of this stone landscape. The initial project involved an extensive survey of the southern wall sections, identifying key preservation issues in the best-preserved area. From 2019, a second project focused on the northern walls, which were severely degraded due to overgrowth. Those areas are particularly afflicted by severe degradation from unchecked vegetation growth. Laser scanning, photogrammetry, and investigations — encompassing historical, archaeological, geological, petrographic, physical-chemical, and numerical studies — were conducted, targeting the Valverde and San Pietro bastions. A pilot site for cleaning and consolidation protocols was also established [4].

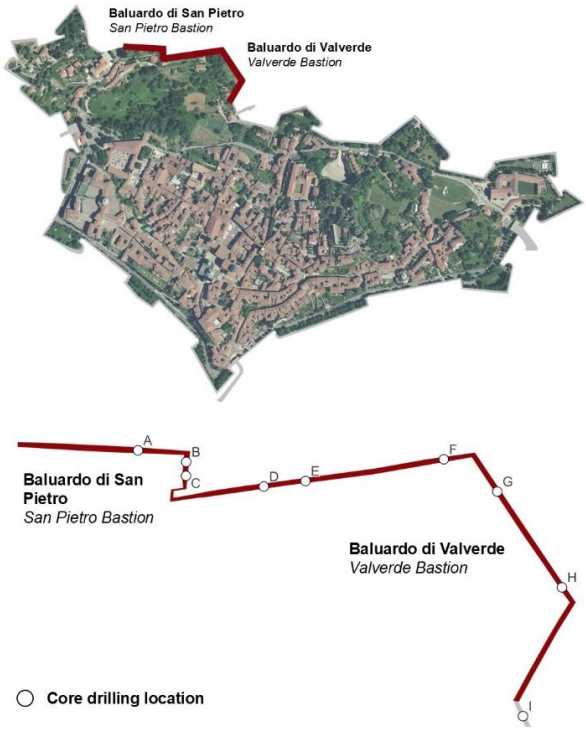

Fig. 1. Plan of the Venetian Fortress of Bergamo, indicating the sampling locations.

During geological surveys, nearly horizontal core samples were extracted from the masonry at the wall base,

allowing verification of wall thickness and providing samples to evaluate the masonry's consistency and composition beyond the surface [4].

II. MATERIALS AND METHODS

Horizontal drillings through the masonry thickness were carried out at an approximate height of 1.50 m above the ground (Figure 2). 9 cores (named from A to I) were extracted, with lengths spanning from 2 to 4 m.

Fig. 2. Core drilling in the masonry carried out by Ecogeo srl.

From the cores, containing parts of mortar, rocks and other fill materials used in the construction, 44 specimens were extracted at different position in the cores, ground and analysed individually. From 3 of the cores, extracted from different zones in the wall (namely core B, D and H) bulk samples, consisting of approximately 250 g of mortar, were collected. Five aliquots were measured for each bulk sample (for a total of 15 XRD patterns) to obtain data on the average mortar composition in the groups.

A. X-ray diffraction (XRD) analysis

X-ray diffraction (XRD) analysis was carried out on the mortar specimens using an X-Ray powder diffractometer Bruker D8 Advance. Measurements were performed in the θ/2θ configuration using Cu Kα radiation (λ = 1.5418 Å), at a voltage of 40 kV and with a current of 40 mA. The diffracted signal was collected using a Lynxeye XE-T® solid-state detector with a 5° window. The scan range was 2-70 °2θ with a step size of 0.01 °2θ and a measuring time of 19 s/step. Millimetre-sized aggregates were separated from the materials before the measurements, then the samples were ground in an agate mortar. Patterns from the 59 samples of mortar (binder and aggregates) were collected and analysed for the identification of the phases. The patterns were analysed using DIFFRACPLUS EVA© version 5.1.0.5 software equipped with the ICDD-PDF (International Centre for Diffraction Data - Powder Diffraction Files) database (version 2024). XRD pattern analysis allowed the identification of the mineralogical phases and the quantification of the abundance of the phases in each sample, by means of semi-quantitative analysis performed with the RIR (Reference Intensity Ratio) method as implemented within the EVA© software. RIRs are a general, instrument-independent constant for use in quantitative phase analysis by the X-ray powder diffraction internal standard method [5]. When the reference standard is corundum, RIR is known as I/Ic. These constants are collected in the ICDD-PDF database. Also, the amorphous content of each sample was determined using the DIFFRACPLUS EVA© internal algorithm in the interval 5-70 °2θ.

B. Principal Component Analysis (PCA)

Multivariate analysis, in the form of principal component analysis, was performed to determine the possible existence of patterns in the mineralogical composition distribution across samples. The input data were the phase abundances obtained from semi-quantitative XRD phase analysis. The 44 measurements of the small mortar samples and the 15 measurements from the bulk samples were analysed separately. Prior to PCA, the abundance data were normalized to include the amorphous fraction, then the obtained values were mean-centered and scaled to unit variance to balance the influence of mineral phases with different abundance ranges. PCA was carried out on the covariance matrix using the software OriginLab OriginPro© 2025b.

III. RESULTS AND DISCUSSION

XRD diffraction analysis was carried out to evaluate crystallinity and identify the phase composition in the mortar. The abbreviations used in the paper for the mineralogical phases are reported in Table 1. The mortars show good cohesion and are predominantly white or light grey colour. The phase composition of all 59 samples was estimated via the RIR (Reference Intensity Ratio) method as implemented within the EVA© software.

A. Phases identification in bulk samples

The mineralogical characterization of the bulk samples from cores B, D and H shows that all three mortars mainly consists of: calcite ($CaCO_3$), quartz (SiO_2), phyllosilicates such as muscovite ($KAl_2(Si_3AlO_{10})(OH)_2$) and clinochlore ($(Mg,Fe)_5Al(Si_3Al)O_{10}(OH)_8$), brucite $Mg(OH)_2$, aragonite ($CaCO_3$), hydration products such as hydrocalumite ($Ca_4Al_2O_6(CO_3)_{0.5}(OH)\cdot 10.75H_2O$) and hydrotalcite ($Mg_6Al_2(CO_3)(OH)_{16}\cdot 4H_2O$), inosilicates such as plombierite ($Ca_5H_2Si_6O_{18}\cdot 6H_2O$), and albite ($NaAlSi_3O_8$). In addition to the crystalline compounds, the mortar contains a large fraction of amorphous phase (18 ÷ 25 wt%). The phases were quantified, and the composition is reported in the heat map of Figure 3 comprising the 15

measurements of the 3 mortars.
Among the identified phases, the following compounds were attributed to the aggregate fraction: quartz (Qu), muscovite (Mu), clinochlore (Cl) and albite (Al), while hydrocalumite (Ca-Hy), hydrotalcite (Mg-Hy), brucite (Br), and plombierite (Pl) are attributed to the binder fraction of the mortar, together with the amorphous fraction (Am).

Table 1. mineralogical phases names, formulae and abbreviations.

Phase Name	Chemical Formula	Abbr.
Calcite	$CaCO_3$	Ca
Quartz	SiO_2	Qu
Muscovite	$KAl_2(Si_3AlO_{10})(OH)_2$	Mu
Hydrocalumite	$Ca_4Al_2O_6(CO_3)_{0.5}(OH)\cdot 10.75H_2O$	Ca-Hy
Aragonite	$CaCO_3$	Ar
Brucite	$Mg(OH)_2$	Br
Clinochlore	$(Mg,Fe)_5Al(Si_3Al)O_{10}(OH)_8$	Cl
Jennite	$Ca_9Si_6O_{18}(OH)_6\cdot 8H_2O$	Je
Hydrotalcite	$Mg_6Al_2(CO_3)(OH)_{16}\cdot 4H_2O$	Mg-Hy
Albite	$NaAlSi_3O_8$	Al
Plombierite	$Ca_5H_2Si_6O_{18}\cdot 6H_2O$	Pl
Vaterite	$CaCO_3$	Va
Dolomite	$CaMg(CO_3)_2$	Do
Ettringite	$Ca_6Al_2(SO_4)_3(OH)_{12}(H_2O)_{24}$	Et
Amorphous	-	Am

Calcite (Ca) instead, was attributed to both the binder and the aggregate fraction. In the binder fraction, calcite is present as the result of the usual carbonatation reaction of portlandite ($Ca(OH)_2$) in the hardening reaction of lime binders: $Ca(OH)_2 + CO_2 \rightarrow CaCO_3 + H_2O$. Meanwhile, a large fraction of the aggregates is constituted by a typical calcareous local black sand. Petrographic observations (not reported here) and XRD measurements on a fragment of the black sand confirm this mineralogical composition. (see Section III-B).
The XRD phase quantification in the bulk samples suggests good control of the mix design for the mortars. Indeed, in all the bulk samples of core B, D and H, the same 10 phases could be detected. Small differences are to be found in the higher amount of quartz and the absence of plombierite in the sample from core B, a slightly larger abundance of calcite in core D, and a larger amount of hydrated phases and of the amorphous fraction in core H (Figure 3).

B. Phases identification in individual mortar samples

The analyses of the specimens collected throughout all the cores in small portions (a few cm^3) show as expected a much larger variation in the number of phases and in their amounts. The corresponding heatmap is reported in Figure 4.

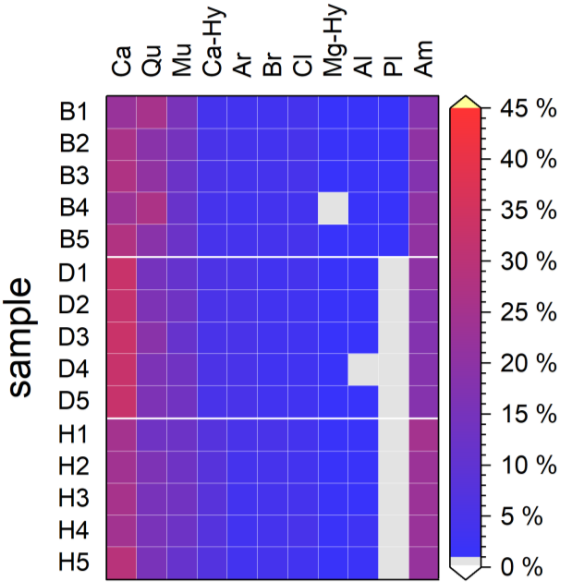

Fig. 3. Heat map of wt% composition of bulk mortar samples. On the top axis the phases are reported with abbreviations detailed in section III.A. (amount increases from blue to red according to the colour scale reported on the right; gray: < 1%, white: phase not detected; yellow: >45%).

The identified compounds are: calcite ($CaCO_3$), quartz (SiO_2), muscovite ($KAl_2(Si_3AlO_{10})(OH)_2$) and clinochlore ($(Mg,Fe)_5Al(Si_3Al)O_{10}(OH)_8$), brucite ($Mg(OH)_2$), aragonite ($CaCO_3$), hydrocalumite ($Ca_4Al_2O_6(CO_3)_{0.5}(OH)\cdot 10.75H_2O$), hydrotalcite ($Mg_6Al_2(CO_3)(OH)_{16}\cdot 4H_2O$), plombierite ($Ca_5H_2Si_6O_{18}\cdot 6H_2O$) and albite ($NaAlSi_3O_8$). Also, jennite ($Ca_9Si_6O_{18}(OH)_6\cdot 8H_2O$) a crystalline form of calcium silicate hydrate, vaterite ($CaCO_3$), a metastable polymorph of calcium carbonate, dolomite ($CaMg(CO_3)_2$) and ettringite ($Ca_6Al_2(SO_4)_3(OH)_{12}(H_2O)_{24}$) were detected sporadically in a few samples. The amount of the amorphous fraction (Am) was quantified in a range from 14 to 27% by weight of the analysed fragments (only exception is sample D30pn with Am<3%). Many of the fragments show a consistent composition, not far from that of the bulk samples, but a few outliers were also observed. Those are to be explained partially by the choice of the operator to collect and analyse specimens with a peculiar visual aspect. Examples of those kinds of samples are sample A-10, F-05a, F-09 and G-08 that contain a large amount of brucite (to be found concentrated in a collection of white lumps evenly distributed in the mortar). Samples D-28a, F-05a, F-09, H-36b and I-11 have a large amount

of aragonite. Samples H-16, I-13a and in a lesser extent I-13b and G-08, contain a large fraction of jennite.

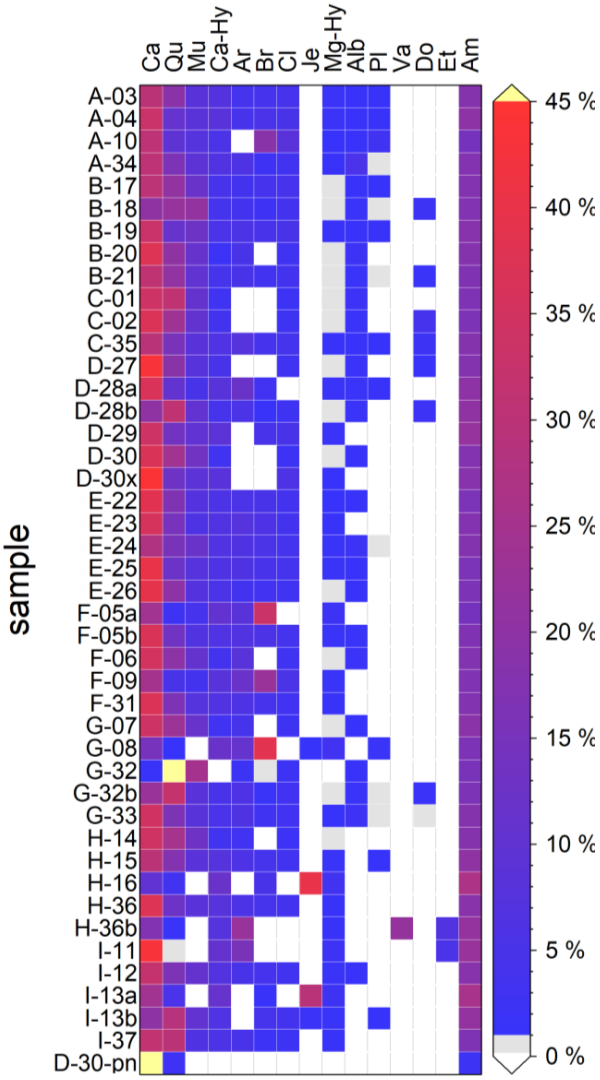

Fig. 4. Heat map of wt% composition of individual mortar samples. On the top axis the phases are reported with abbreviations detailed in section III.B. (amount increases from blue to red according to the colour scale reported on the right; gray: < 1%, white: phase not detected; yellow: >45%).

Unlike the other specimens, sample D-30pn was intentionally chosen to include a large fragment of black sand aggregate, therefore it does not reflect the mortar composition. The analysis shows that it is mainly constituted of calcite, supporting the claim in Section III-A about the distribution of calcite in both the binder and the aggregate.

C. PCA analysis

PCA analysis was performed on the bulk samples and on the individual samples separately.

Starting from the bulk samples, in Figure 5 the biplot is presented. The vectors represent the mineralogical phases and reflect the co-variance of the phases in the specimens; the first two principal components account for nearly 69% of the total variance. The half-filled circles represent the scores of the individual samples and reflect their composition. The shaded shapes represent the 95% confidence ellipsoids.

The loading graph shows that the amorphous content (Am), hydrotalcite (Mg-Hy) and hydrocalumite (Ca-Hy) phases and brucite (Br) amounts are positively correlated, being phases that develop in the hydration of the binder. PCA reveals a strong correlation between aragonite and calcite. The matter is complicated by the fact that calcite is part of both the carbonatated binder and the calcareous aggregate.

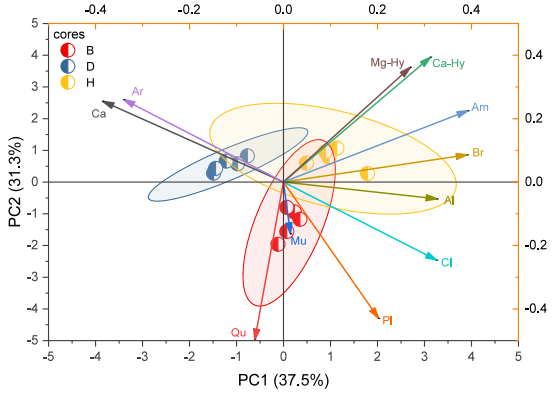

Fig. 5. Biplot of PCA analysis of phases abundance in bulk samples of cores B, D and H.

Literature suggests that aragonite is commonly formed as a metastable phase in hydraulic lime binders [6] [7] [8], therefore it is expected to be found in association with the calcite produced during the hardening and ageing of the binder. Further analysis could be required to disentangle these contributions. The differences in phase composition that were noticeable in the heatmap emerge also from the bi-plot. A slight clustering is observed among samples, based on core origin, (core B, core D and core H). core H is more associated with hydration products and amorphous content. In contrast, and quartz (Qu) and muscovite (Mu) show negative loadings, indicating a stronger presence in cores B and D. Overall, despite some internal dispersion, the confidence ellipses overlap significantly, indicating no distinct clustering by sampling location. This supports the interpretation of a relatively homogeneous phase distribution across the two studied bastions

PCA performed on individual small samples reveals a more scattered distribution of mineral phases compared to previous analyses on composite samples. This discrepancy likely reflects the influence of local heterogeneities and sampling bias in small-scale specimens, which may not

capture the full compositional spectrum of the mortar. In contrast, composite samples—obtained by averaging multiple aliquots—tend to smooth out local variations, resulting in more stable phase correlations. The biplot relative to the PCA analysis based on cores (representative of the different drilling positions) is presented in Figure 6.

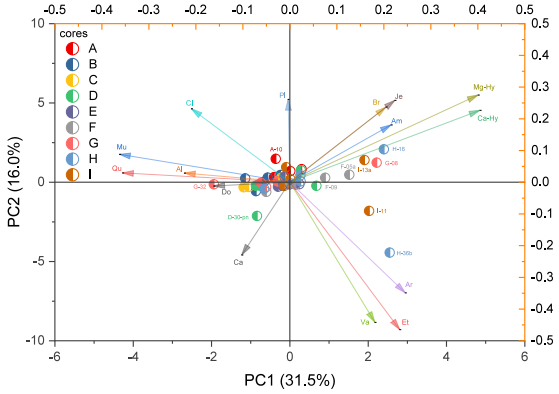

Fig. 6. Bi-plot of PCA analysis of phases abundances in individual samples, grouped by core (A to I).

In this situation, the first two principal components only account for 47.5 % of the total variance, indicating the complexity of the phase relations in the dataset.

The loading graph highlights the strong internal correlation of the hydrated phases in the binder (Am, Ca-Hy, Mg-Hy, Br and Je) and among the aggregate-related phases (Qu, Mu, Al, Do), and their strong negative correlation. This pattern is likely due to sampling bias, where binder-rich or aggregate-rich mortar samples were selected. Calcite, being present in both the subsets, ends up poorly correlated, while the metastable carbonates vaterite and aragonite show a strong association.

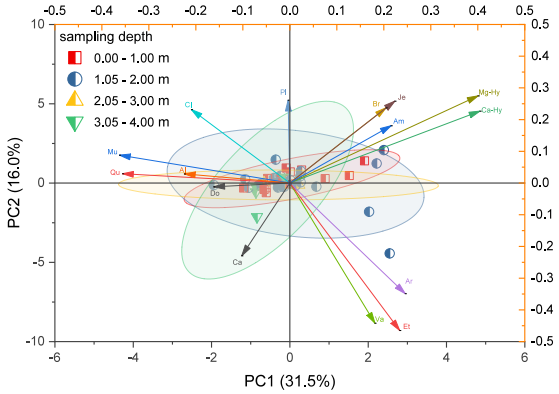

Fig. 7. Bi-plot of PCA analysis of phases abundances in individual samples, grouped by sampling depth (1 to 4m).

The sample scores, here grouped by the core, are largely clustered in the centre, with no dispersion whatsoever. The confidence ellipsoids are not shown for sake of clarity, since they are nearly completely overlapped to each other. The few individual samples that stand-out are indicated on the graph and are those mentioned above in Section IIIB for having a peculiar composition.

The bi-plot reported in Figure 7 groups the samples for sampling depth (0.00-1.00 m, 1.05 – 2.00m, 2.05-3.00 m, 3.05-4.00 m). No clustering is apparent either, as witnessed by the complete overlapping of the confidence ellipsoids.

IV. CONCLUSIONS

The historic mortars of the wall of Venetian Fortress of Bergamo were analysed by means of X-ray diffraction and the results were analysed using PCA. Mineral phases present in the mortar were identified and associated with the binder and aggregate fractions. The main crystalline compounds are calcite, quartz, muscovite, hydrocalumite-type and hydrotalcite-type compounds, brucite, aragonite, plombierite, clinochlore and albite. Also, jennite, vaterite, dolomite and ettringite were identified occasionally. Additionally, the mortar contains a large fraction of amorphous phases (between 14 and 27 wt%). The results of PCA on composite samples—obtained by averaging multiple aliquots—tend to smooth out local variations, resulting in more stable phase correlations. Overall, the PCA analysis confirms a relatively homogeneous mineralogical composition across the cores, indicating that the binder composition remains consistent across the examined portions of the wall.

V. REFERENCES

[1] G. Labaa, «Parti ed elementi delle mura venete», in *Le mura di Bergamo*, Azienda autonoma di turismo, Bergamo, 1977, pp. 169–178.

[2] P. Capellini, «Le mura dopo il dominio veneto», in *Le mura di Bergamo*, Azienda autonoma di turismo, Bergamo, 1977, pp. 325–348.

[3] World Heritage Committee, «Nominations to the World Heritage List 2017», UNESCO, 2017. [Online]. Disponibile su: https://whc.unesco.org/archive/2017/whc17-41com-8B-en.pdf

[4] D. Marsetti, «Indagine geognostica geologica», in *Il baluardo di Valverde: una ferita da ricucire nella fortezza veneziana di Bergamo.*, Comune di Bergamo, 2020, p. 176.

[5] C. R. Hubbard and R. L. Snyder, «RIR - Measurement and Use in Quantitative XRD», *Powder Diffr.*, vol. 3, fasc. 2, pp. 74–77, giu. 1988, doi: 10.1017/S0885715600013257.

[6] G. Ricci *et al.*, «The Cannero Castle (Italy): Development of Radiocarbon Dating Methodologies in the Framework of the Layered Double Hydroxide Mortars», *Radiocarbon*, vol. 62, fasc. 3, pp. 617–631, 2020, doi: 10.1017/RDC.2020.31.

[7] M. Shivakumar and T. Selvaraj, «Characterization study on the influence of limestone and shell lime as

a fine aggregate substitute: A traditional approach on lime plaster restoration», *Mater. Today Proc.*, vol. 45, pp. 6519–6526, 2021, doi: 10.1016/j.matpr.2020.11.454.

[8] M. D. Jackson *et al.*, «Phillipsite and Al-tobermorite mineral cements produced through low-temperature water-rock reactions in Roman marine concrete», *Am. Mineral.*, vol. 102, fasc. 7, pp. 1435–1450, 2017, doi: 10.2138/am-2017-5993CCBY.

VI. FUNDING

This work has been supported by Fondazione Cariplo, grant [n° 3068-2019, call 2019] “Arte e Cultura - Beni al sicuro”.